Sensitivities of subgrid-scale physics schemes, meteorological forcing, and topographic radiation in atmosphere-through-bedrock integrated process models: A case study in the Upper Colorado River Basin

5 Zexuan Xu[1], Erica R. Siirila-Woodburn[1], Alan M. Rhoades[1], Daniel Feldman[1]

[1] Earth and Environmental Sciences Area, Lawrence Berkeley National Laboratory

Correspondence to: Zexuan Xu (zexuanxu@lbl.gov)

Abstract. Mountain hydrology is controlled by interacting processes extending from the atmosphere through the bedrock.
10 Integrated process models (IPM), one of the main tools needed to interpret observations and refine conceptual models of the mountainous water cycle, require meteorological forcing that simulates the atmospheric process to predict hydroclimate then subsequently impacts surface-subsurface hydrology. Complex terrain and extreme spatial heterogeneity in mountainous environments drive uncertainty in several key considerations in IPM configurations, and require further quantification and sensitivity analyses. Here, we present an IPM using the Weather Research and Forecasting (WRF) model coupled with an
15 integrated hydrologic model, ParFlow-CLM, implemented over a domain centered over the East River Watershed (ERW), located in the Upper Colorado River Basin (UCRB). The ERW is a heavily-instrumented 300 km^2 region in the headwaters of the UCRB near Crested Butte, CO, with a growing atmosphere-through-bedrock observation network. Through a series of experiments in water year 2019 (WY19), we use four meteorological forcings derived from commonly used reanalysis datasets, three subgrid-scale physics scheme configurations, and two terrain shading options within WRF to test the relative
20 importance of these experimental design choices on key hydrometeorological metrics including precipitation, snowpack, as well as evapotranspiration, groundwater storage, and discharge simulated by the ParFlow-CLM. Results reveal that sub-grid scale physics configuration contributes to larger spatiotemporal variance in simulated hydrometeorological conditions, whereas variance across meteorological forcing with common sub-grid scale physics configurations is more spatiotemporally constrained. For example, simulated discharge shows greater variance in response to the WRF simulations across subgrid-
25 scale physics schemes (26%) rather than meteorological forcing (6%). Topographic radiation option has minor effects on the watershed-average hydrometeorological processes, but adds profound spatial heterogeneity to local energy budgets (+/-30 W/m^2 in shortwave radiation and 1 K air temperature differences in late summer). The findings from this study provide guidance on an IPM setup that most accurately represents atmospheric-through-bedrock hydrometeorological processes and can be used to guide future modeling and fieldwork in mountainous watersheds.

1. Introduction

An improved predictive understanding of watershed dynamics and response to perturbations is particularly important for mountainous watersheds due to the multitude of natural services they provide even while those services are highly vulnerable to anthropogenic and natural environmental change (Hubbard et al., 2018; Siirila-Woodburn et al., 2021). The Upper Colorado River Basin (UCRB), which supports 40 million people and ecosystems that has experienced major hydrological change in recent decades (James et al., 2014). Discharge may have decreased by ~9.3% per degree Celsius of warming, due to processes extending from the atmosphere through the subsurface (Milly and Dunne, 2020). Drought is common to the region, however, the current multi-decade drought is unprecedented in at least the last 1200 years (Williams et al., 2022). To better estimate how aridification of the UCRB might continue, processes that shape the water cycle in this region must be considered holistically, including atmospheric processes such as large-scale vapor transport, precipitation and radiation, land surface processes such as evapotranspiration and snowpack metamorphosis, and surface-through-subsurface hydrological processes. Atmospheric and land surface processes all interact and influence river discharge through riverine processes, infiltration, and subsurface flow and storage, but their impact varies depending on the temporal and spatial scales of analysis (Siirila-Woodburn et al., 2021). Unfortunately, there is a dearth of observational data to constrain these processes at their relevant scales, leading to persistent biases in the predictive understanding of the mountainous hydrologic cycle with direct implications for water resource management (Sturm et al., 2017; Rhoades et al., 2018a,b,c; Xu et al., 2019). A recent study by Lundquist et al. (2019) highlighted that calibrated models, which themselves have numerous deficiencies, have likely outpaced the skill of observationally-based gridded products in advancing the understanding of the integrated mountainous hydrologic cycle. Fortunately, observational campaigns, combined with coordinated modeling activities, represent a potential path forward towards enhancing our predictive understanding of the hydrologic cycle in complex terrain (Feldman et al., 2021).

Here, we explore how modeling activities can best support that path forward. Process models provide an essential tool for quantifying linear and non-linear interacting processes across spatiotemporal scales that arise in mountains and can help to fill observational gaps. However, the processes that are represented in these process models are a mixture of fundamental physics and subgrid-scale parameterizations, many of which were not developed with mountainous hydrologic cycle processes in theory, and/or are based on decades-old field and laboratory data. To further compound those issues, cross-scale interactions in complex terrain are challenging to resolve at their native scales with currently available advanced computing resources (Siirila-Woodburn et al., 2021). While discipline-specific process models, such as those used to explore and predict atmospheric or subsurface processes have advanced scientific understanding in a myriad of ways through sustained engagement with extensive user communities (Gutowski et al., 2020), Integrated Process Models (IPMs), in which these discipline-specific process models are coupled, are relatively novel and are still being vetted for various scientific applications in complex terrain. For example, Maina et al. (2020) explored how the horizontal resolution of atmospheric

forcings (40km to 0.5 km) in the Cosumnes River watershed, California, simulated by a widely-used regional climate model
(Weather Research and Forecasting (WRF; Powers et al., 2017), result in differences in surface and subsurface hydrologic
65   metrics when used to force the integrated hydrologic model (ParFlow-CLM; Maxwell et al., 2015). We expand that
sensitivity analysis in this study, including model meteorological forcing and subgrid-scale physics configuration choice, and
their influence on the surface-through-subsurface response of the integrated hydrologic model. The goal of this work is to
provide the mountain hydrology research community with a properly-configured IPM that can inform ongoing and future
field campaigns and their process-modeling needs in the UCRB.

70

Standalone WRF simulations have been widely investigated in complex terrain, and provide context for the unfilled gaps in
IPM investigation and development in complex terrain. For example, several papers detailed the role of subgrid-scale
physics configuration on precipitation and snowpack processes in the UCRB (Rasmussen et al., 2011; Liu et al., 2011; Liu et
al., 2017; Rasmussen et al, 2020). Outside of the UCRB, Orr et al. (2017) found cloud microphysics schemes have
75   significant impacts on monsoon precipitation simulation in the complex-terrain Himalayan regions, with the Morrison
microphysics scheme producing the best agreement with observations. Conversely, Comin et al. (2018) found that the
Morrison microphysics scheme produced excessive snowfall and exhibited poor performance when evaluated in the Andes,
while the Goddard (WDM6) scheme exhibited the best performance with respect to observed snowfall. In terms of land
surface process, Jin et al. (2010) explored that land surface model complexity improves temperature simulation, but has a
80   minimal impact on simulated precipitation. Additionally, Mallard et al. (2017) evaluated that the sensitivity of near-surface
temperatures and precipitation to changes in land use representation is smaller than the model error for those fields, while
Rudisill et al., (2021) found that the details of snow cover in the initial conditions of a WRF simulation in complex terrain
are key to ensuring the skill of that simulation, not just in 2-meter air temperature but also in the surface energy budget.
Meanwhile, Rahimi et al (2022) found minimal sensitivity of SWE in WRF simulations across the entire western United
85   States to microphysics schemes, but found large effects due to model resolution. On the other hand, the effects of
meteorological forcing as the lateral boundary conditions of WRF simulations have also been recognized. For instance, Xu et
al. (2018) identified that the simulations of hydroclimate in California using WRF are largely driven by large-scale forcing
datasets. Taken together, the published literature suggests a one-size-fits-all WRF model configuration for hydrological
studies in complex terrain may not be possible. In other words, the WRF configuration is likely case- and region-specific,
90   and could depend either on the representation of processes within the WRF simulation domain or the boundary conditions of
WRF forced by the large-scale meteorological forcing. The options of subgrid-scale physics schemes and large-scale
meteorological forcing datasets need to be fully tested to understand their sensitivities to atmospheric and hydrological
processes in the ERW.

95   Furthermore, few studies have assessed how these choices impact the subsequent simulation of surface-through-subsurface
hydrologic processes. These types of analysis are needed because the WRF model can be configured in myriad ways for a

given domain, and feedbacks to the surface and subsurface hydrology can yield a potentially large range of results. The aforementioned IPM study by Maina et al. (2020) showed that biases of 5-10% in basin-average surface water storage can result from forcing resolution differences in WRF alone, with localized differences in groundwater head by several meters.

100 Schreiner-McGraw and Ajami (2020) show that water partitioning across four commonly used meteorological forcings differs substantially within a Sierra Nevada watershed, and that the combination of precipitation uncertainty, soil parameterization, and topographic position all impact the severity to which these differences in forcing exert on the hydrology.

105 In spite of the range of WRF sensitivity investigations, the connections between uncertainty in a WRF configuration and its influence on surface-through-subsurface hydrology is underexplored and therefore the focus of this work. It should be noted that our investigation is not to explore general principles behind IPM uncertainty quantification and error propagation, but rather to present a concrete use-case to guide the advancement of atmosphere-through-bedrock modeling and its connections to mountainous hydrological science. Using an IPM, we address an outstanding question: does synoptic-scale meteorological

110 forcing or meso-to-micro scale atmospheric processes have a more direct effect on surface and subsurface hydrologic processes in a mountainous watershed?

In order to answer this question, we undertake a series of experiments with different synoptic-scale meteorological forcings, and different, plausible choices for meso-to-micro scale parameterizations in the IPM. This is informed by prior standalone

115 WRF studies that have utilized different shortwave and longwave radiation, microphysical, and surface and planetary boundary layer schemes (Skamarock et al., 2019). Additionally, topographical shortwave shading effects are tested to understand how spatial heterogeneity in the surface radiation budget influences evapotranspiration and snowpack accumulation and ablation processes (Arthur et al., 2018). Then we explore how the surface and subsurface hydrology fields respond to these various experimental setup choices, especially discharge in the ERW of the UCRB (described below). With

120 a discrete set of simulations, we establish the relative importance of these choices. We can also establish the relative importance of subgrid-scale parameterizations that affect water and energy budgets. Our hypothesis is that if synoptic-scale forcings produce a much larger spread in surface and subsurface hydrology fields than subgrid-scale physics scheme choice, then predictive hydrology in the UCRB should prioritize improving large-scale weather products and analyses. Conversely, if model subgrid-scale physics scheme choice produces more variability in hydrologic response, then smaller scale

125 atmospheric and hydrological processes affected by surface heterogeneity in the ERW should be prioritized for model development. Finally, we can establish if there are spatial and/or temporal patterns to differences between models and observations that point to model configuration choices and thereby motivate further, directed model development and sensitivity studies.

130 Therefore, this article is organized as follows: first, we present details of study site and hydroclimate in the water year, as
well as the IPM including the coupling between WRF and ParFlow-CLM and the justifications for using WRF and ParFlow-
CLM as the atmospheric and surface-through-subsurface process models in the IPM, respectively. Then, we describe the
WRF experiments that we performed to test the relative importance of synoptic-scale boundary forcing and meso-to-micro
scale model subgrid-scale physics schemes for driving ERW integrated hydrological simulations. Next, we present the

135 simulated discharge, evapotranspiration and groundwater storage using ParFlow-CLM, to quantify the responses to changing
WRF configurations. We conclude by contextualizing these results in light of the ongoing field campaign activities in the
ERW.

2. Study Site

This investigation focused principally on modeling and analysis of the ERW, a representative mountainous headwater

140 catchment of the UCRB near Gothic, Colorado (Hubbard et al., 2018). This 300 km^2 watershed of the Upper Colorado River
Basin is at a high-level, representative of the UCRB that it has very large gradients in precipitation (e.g., a factor of 2 range
in precipitation between the northern and southern boundary of the ERW) and surface-through-subsurface hydrology. The
ERW has a continental, subarctic climate with long, cold winters and short, cool summers. At an average elevation of 3266
meters above sea level, the watershed has a mean annual temperature of 0°C, and distinct winter and growing seasons that

145 influence hydrologic and biogeochemical cycles. River discharges are driven primarily by snowmelt in late spring to early
summer, with mid- to late-summer monsoonal rainfall inducing rapid but punctuated increases in streamflow. The ERW
receives ~1200 mm/yr of precipitation and we focus here on Water Year 2019 (Oct 1, 2018 - Sep 30, 2019).

The ERW has become a mountainous community testbed for improving predictive understanding of multi-scale atmosphere-

150 through-bedrock system dynamics and is the centerpiece of such focused activities because it is one of two major tributaries
that form the Gunnison River, which in turn accounts for near half of the Colorado River's discharge at the Colorado–Utah
border. In the past decade, several synthesis research efforts have been established in this region, including a wide range of
fieldwork and modeling activities (Hubbard et al., 2018). The ERW has become one of the most heavily-instrumented
mountainous watersheds in the world, which makes it an ideal focus for this research given the potentially large number of

155 observational constraints available for the IPM efforts presented here.

3. Methods

3.1. WRF models

The Weather Research & Forecasting (WRF) model version 4.0 is used in this study (Powers et al., 2017). WRF was chosen because of its widespread use in the investigation of atmospheric and land processes, and contextualizing observations in
160   complex terrain (Rasmussen et al., 2011; Rasmussen et al., 2014). The WRF model is comprised of a fully coupled atmospheric and land surface model with a range of user-specific options for subgrid-scale physics schemes. WRF is a regional climate model that requires boundary and initial conditions provided by either global climate model (GCM) outputs or atmospheric reanalyses datasets. Our configuration of the WRF model is designed with three nested domains, with an outer, middle and inner domains at grid resolution of 4.5 km, 1.5 km and 0.5 km, respectively, centered around Crested
165   Butte, Colorado where the East River watershed is located (Figure 1).

While the stand-alone WRF model has been used extensively to advance the understanding of atmospheric processes, it has lower fidelity and applicability to investigate surface-through-subsurface hydrologic processes, and therefore is limited as an assessment tool for understanding integrated mountainous hydrologic cycle. Therefore, to provide an estimate of the entire
170   hydrologic budget, we use a one-way coupling between WRF and an integrated hydrologic model, ParFlow-CLM (Maxwell et al., 2015, described in further detail below), in order to simulate the hydrological response of key variables not otherwise quantifiable in standalone WRF, such as discharge and groundwater storage.
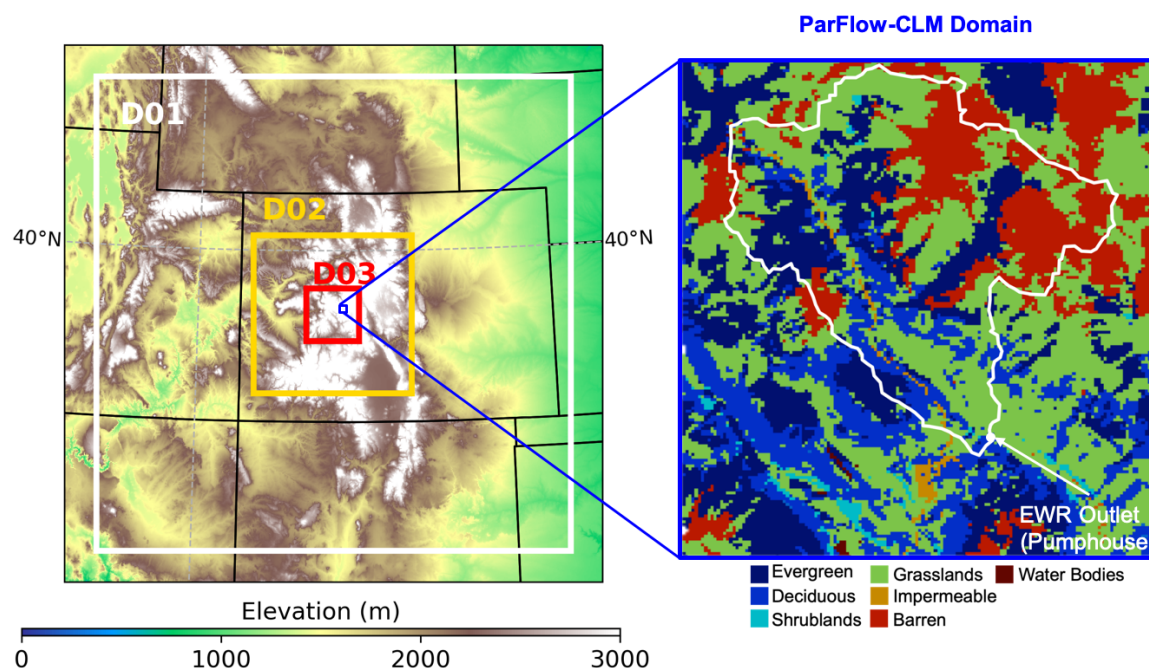
175   ***Figure 1**. Left: Three nested WRF domains D01 (4.5 km grid resolution, 201 by 201 grid cells or 900 by 900 km extent), D01 (1.5 km grid resolution, 201 by 201 grid cells or 300 by 300 km extent), and D03 (0.5 km grid resolution, 201 by 201 grid*

cells or 100 by 100 km extent) and their associated elevations (left). The Global Multi-resolution Terrain Elevation Data 2010 (GMTED2010) elevation data in meters above mean sea-level is used in the WRF simulation. Right: the innermost ParFlow-CLM domain and spatial extent of the East River Watershed (white line) and associated land cover type derived
180 *from the National Land Cover Dataset (NLCD) (Homer et al, 2020) and upscaled to 100 m (right).*

A major experimental design decision when simulating the integrated mountainous hydrologic cycle is computational cost associated with the throughput of the simulations (e.g., simulated years per actual day) that are determined by model horizontal, vertical, and timestep resolutions and subgrid scale physics parameterization complexity. Computational
185 expenses for exploring the sensitivities of WRF configuration choice in this study were significant: one simulated year requires approximately 100,000 CPU hours on LBNL's Lawrencium lr6 supercomputing system. As such, it was highly impractical to simulate the entire configuration space of meteorological forcing and subgrid-scale parameterization choice. A discrete sub-sample of configurations, as presented here, is used to isolate and systematically determine which combination of subgrid scale parameterization choice is superior for a given domain such as the ERW. We therefore adopted a
190 parsimonious approach to explore the space of possible WRF configurations, described below.

3.1.1. Subgrid-scale physics schemes

Three well-established suites of subgrid scale physics schemes for WRF are evaluated in this study (Table 1). One scheme was developed by NCAR and is used for a wide range of simulations over domains extending across the entire Conterminous United States (CONUS) (Liu et al., 2017). Another scheme that we consider here has been used for decadal-length
195 hydroclimate simulation over California (Huang et al., 2017; Xu et al., 2018; Ullrich et al., 2018), and since it was initially developed by researchers at the University of California, Davis, it is denoted as UCD here. More recently, Flores et al. (2016) and Rudisill et al. (2021) implemented a WRF configuration that focused on exploring land-atmosphere interactions in complex terrain. This configuration was developed by researchers at Boise State University, and is referred to as BSU here.

200

Table 1: Microphysics, radiation, land surface model, surface layer, and planetary boundary layer schemes used for the three different WRF configurations of the IPM tested here.

Subgrid-scale physics schemes	NCAR (CONUS)	BSU	UCD
Microphysics	Thompson	Thompson	WSM6
Shortwave radiation	RRTMG	RRTM	RRTMG

Longwave radiation	RRTMG	RRTM	RRTMG
Land surface model	Noah	Noah-MP	Noah
Surface layer	Eta similarity	Monin-Obukhov	Revised MM5
Planetary Boundary layer	Mellor-Yamada-Janjic scheme	Mellor-Yamada-Janjic scheme	UW (Bretherton and Park)

3.1.2. Meteorological forcing

205 Each of these WRF configurations must specify a set of initial and lateral boundary conditions at the synoptic scale and, at least in the outer domain, are typically derived from high-resolution atmospheric reanalyses. The reanalysis from the National Centers for Environmental Prediction (NCEP), Climate Forecast System Reanalysis version 2 (CFSR2), The Modern-Era Retrospective analysis for Research and Applications - Version 2 (MERRA2), European Centre for Medium-Range Weather Forecasting Reanalysis version 5 (ERA5) were used in this study.

210

ERA5 is the fifth generation ECMWF atmospheric reanalysis of the global climate on a 30 km grid resolution (Hersbach et al, 2020), and combines model data with observations from across the world into a globally complete and consistent dataset. The CFSR2 is also global and is designed to provide an operational product for forecasting and analysis purposes at 0.3 degree grid resolution (Saha et al, 2010). The CFSR2 data were generated by an advanced assimilation schemes,

215 atmosphere-land-ocean-sea ice coupling, assimilates satellite radiances. MERRA2 is another atmospheric reanalysis based on data assimilation (Gelaro et al., 2017), which is the first long-term global reanalysis to assimilate space-based observations of aerosols and represent their interactions with other physical processes in the climate system. In addition, the NCEP FNL (NCEP, 2000) operational global analysis and forecast data are on a 0.25-degree grid resolution from the Global Data Assimilation System (GDAS) (Kleist et al, 2009). All meteorological forcing datasets are processed at 6-hourly by the

220 WRF Preprocessing System (WPS).

3.1.3 Topographic radiation

Topographic effects for shortwave radiation flux calculations in complex terrain are evaluated (Arthur et al., 2018). One is the "slope_rad" namelist option, which modifies surface solar radiation flux according to terrain slope by correcting it based on the solar zenith angle relative to the local surface normal vector. This adjustment ensures that the solar radiation received

225 at the surface in WRF is consistent with the geometric projection of incoming sunlight onto local, non-flat surfaces. The other namelist option, "topo_shading", allows for shadowing of neighboring grid cells. When "topo_shading" is active, WRF determines if any topography intersects a line drawn between a given grid point and the location of the sun at the time-step of the WRF run. If so, a topographic shadow is cast on that grid point and the direct component of the incoming solar

radiation is set to 0. In this study, simulations in which "slope_rad" and "topo_shading" are jointly enabled are termed
230   "3DRad" and when jointly disabled are termed "no3DRad", in the inner domain of the WRF simulation.
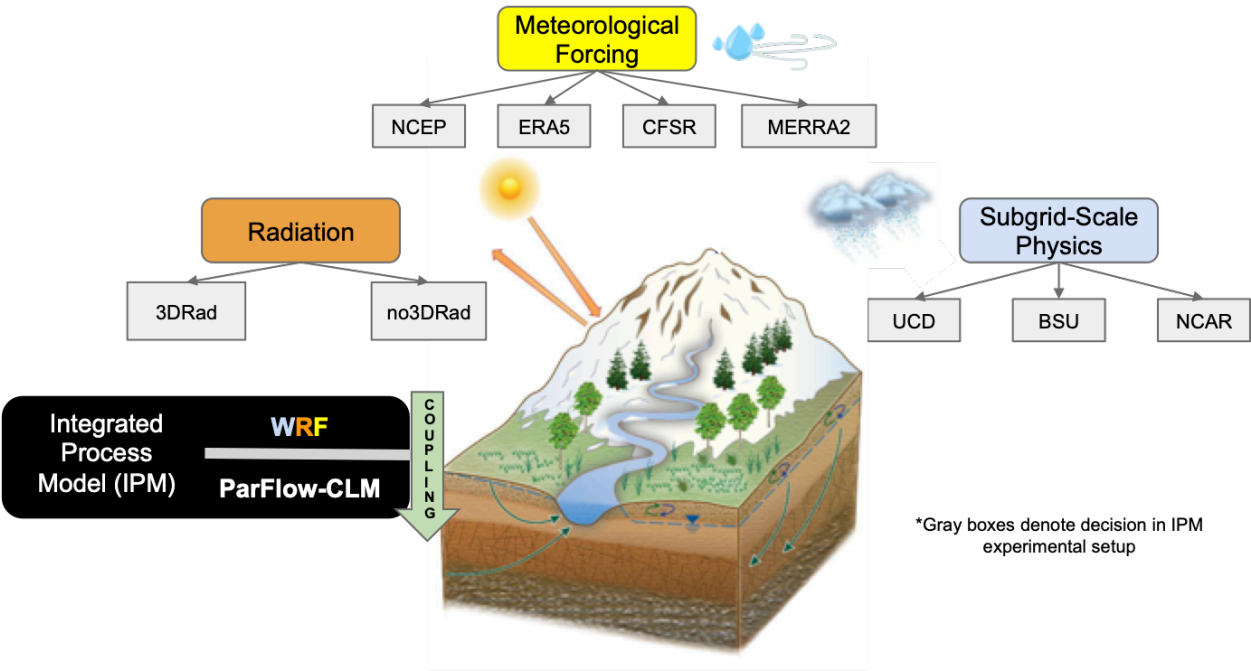
Figure 2. Conceptual framework for developing a set of different WRF configurations of the IPM to evaluate the sensitivities of subgrid-scale physics parameterization choice, meteorological forcing, and radiation scheme in the representation of
235   *mountain water and energy budgets.*

Table 2: East River Watershed WRF experiment configurations. Three subgrid-scale physics schemes, four meteorological forcings, and the topographic radiation options were assessed.

Subgrid-scale physics schemes	Meteorological forcing	Topographic radiation
BSU	CFSR2	3DRad_inner
		no3DRad_inner
	ERA5	3DRad_inner
		no3DRad_inner
	MERRA2	3DRad_inner
	NCEP	3DRad_inner

UCD	CFSR2	3DRad_inner
	ERA5	3DRad_inner
NCAR	CFSR2	3DRad_inner
	ERA5	3DRad_inner

3.2 ParFlow-CLM description

240   ParFlow is a physically based surface-subsurface hydrologic model that solves the coupled flow of saturated and variability-saturated groundwater and overland surface water (Ashby and Falgout, 1996; Jones and Woodward, 2001; Maxwell, 2013). The three-dimensional form of Richards equation is used to solve for lateral and vertical groundwater flow in the subsurface and the kinematic wave approximation is used to solve two-dimensional overland flow. ParFlow is coupled to the land surface model, the Common Land Model (CLM), which calculates a coupled water energy balance at every surface cell of

245   the domain (Dai et al., 2003) and incorporates spatially distributed vegetative processes by including specified land use types parameterized by the International Geosphere-Biosphere Program standard database. Hourly meteorological forcing derived from WRF drives ParFlow-CLM, and includes the following eight variables: precipitation, two-meter surface air temperature, longwave radiation, shortwave radiation, 10-meter east-west and south-north wind speeds, atmospheric pressure, and specific humidity. Computational expenses for ParFlow-CLM are also less substantial than that of WRF for

250   this model configuration, but still require high performance computing. Excluding the time for a multi-year initial condition spinup, a single water year of the ParFlow-CLM simulations on 64 cores on the NERSC's Cori supercomputing system is approximately 1,000 CPU hours.

3.3 Reference Datasets

The Parameter-elevation Relationships on Independent Slopes Model (PRISM) dataset (Daly et al., 2008) was used as the

255   reference dataset to assess model performance of precipitation and temperature in this study. PRISM uses observations from quality-controlled meteorological stations along with a topographic correction method against elevation based on empirical regression to create daily gridded 800-meter total precipitation, and daily average, minimum and maximum two-meter surface temperature.

260   Snowpack Telemetry (SNOTEL) data have been widely used in snowpack assessment (Serreze et al, 1999; Fassnacht et al, 2003), and we use three SNOTEL stations (Butte, Schofield Pass, Upper Taylor) within the WRF inner domain to assess the snowpack simulation skill of each IPM configuration. Significant heterogeneity is sampled by the three SNOTEL stations (within or near the ERW) due to the complex topography. For example, the Butte station is located downstream of the ERW and, on average, receives approximately 0.8 m of precipitation, and reaches 0.4 m in maximum snow water equivalent over

265   the year. On the other hand, the Schofield Pass station is located upstream of the ERW and, on average, receives 1.2 m of precipitation and reaches 0.9 m in maximum snow water equivalent. In addition, we use the snow water equivalent product of the Airborne Snow Observatory (ASO; Painter et al, 2016) on 04/07/2019 to evaluate the spatial pattern skill of the snowpack simulation across WRF configurations (Figure S-6). Notably, ASO SWE estimates are lower than SNOTEL SWE measurements (ASO: 389 mm at Butte, 938 mm at Schofield Pass; SNOTEL: 490 mm at Butte, 1260 mm at Schofield Pass).

270   In addition to SNOTEL station data, stream gauges measurement of discharge at the pumphouse, the outlet of the ERW, is used to evaluate the ParFlow-CLM simulation results.

4.   Results

We start by presenting a number of time-series of spatial averages over the ERW for WY19. They indicate the gross performance of the IPM across the water year, and whether a configuration produces generally reasonable estimates relative

275   to observational products. Figure 3 shows cumulative precipitation, two-meter surface air temperature, and snow water equivalent (SWE). For cumulative precipitation, each configuration produces amounts higher than PRISM (cumulative precipitation of 1201 mm), and the UCD simulates the highest cumulative precipitation. For surface air temperature, the seasonal cycle and daily variability are captured by all configurations, however, exhibit systematic cold biases relative to PRISM (annual average two-meter surface air temperature of 0.6 degrees Celsius). In terms of SWE, all model

280   configurations concur in their representation of the snowpack accumulation season and melt season in late spring and into summer, except UCD which simulates an earlier peak timing of SWE.

The spread in cumulative precipitation when comparing across different meteorological forcing dataset is apparent (Figure 3). Although UCD and NCAR configurations show greater difference in precipitation forced by ERA5 and CFSR2, the

285   consistency across BSU configurations is notable, which also shows the closest agreement with PRISM. When comparing the relative roles of subgrid-scale physics scheme choice to meteorological forcing, the percent difference of cumulative precipitation, calculated with (maximum - minimum)/minimum*100, across BSU-CSFR2, UCD-CSFR2 and NCAR-CSFR2 schemes is nearly 34% of the mininum cumulative precipitation simulated by BSU-CFSR2, compared to the 4.6% of the simulations across BSU configurations with different meteorological forcing (CSFR2, ERA5, MERRA2 and NCEP).

290

BSU simulations are generally in agreement with PRISM. However, the UCD simulations are outliers relative to the other simulations, with cumulative precipitation of 1706 mm, or 42% higher at the end of the water year, with the most notable differences occurring in March through September. NCAR simulations show general agreement with PRISM and BSU throughout the water year, save for June through September. The two-meter surface air temperature time-series reveals that

295   the UCD simulation is systematically colder throughout the winter and spring, regardless of which meteorological forcing dataset is used. The persistent cold bias simulated by the UCD, NCAR and BSU schemes has been found in previous WRF

studies within western US mountain regions (Xu et al., 2018, Rudisill et al. 2021). The SWE time-series again shows a similar relationship with precipitation, with the outlier being UCD-ERA5, in terms of the seasonal timing of when snowpack peaks and melts (Figure S-4).

300
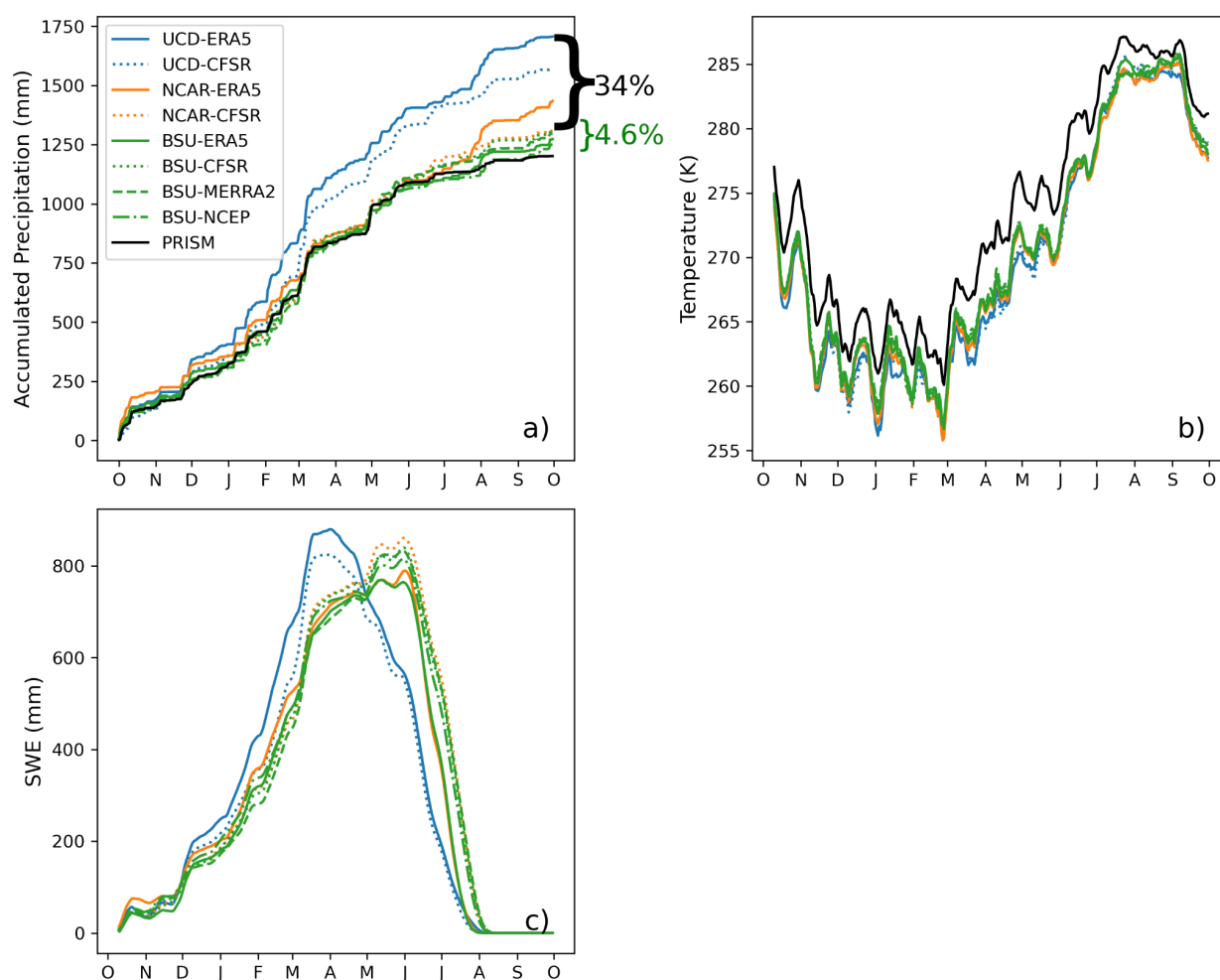
Figure 3. *Cumulative precipitation, two-meter surface air temperature and snow water equivalent (SWE) simulated within the ERW using an IPM with different subgrid-scale physics schemes and meteorological forcings. The cumulative*
305 *precipitation and temperature results are compared relative to PRISM. 10-day moving averages of daily temperature are shown in b). The percent difference in cumulative precipitation across subgrid-scale physics schemes (black brackets) and meteorological forcing (green brackets), calculated by (maximum - minimum)/minimum*100, are provided on the right y-axis.*

310 In addition to the domain-averages, spatial heterogeneity due to land-surface cover and topographic effects are shown in Figure 4. The systematic cold bias simulated throughout the water year appears to be an elevation-dependent phenomena with higher-elevations exhibiting an enhanced cold bias compared with PRISM. However, the river valley and relatively lower-elevation areas at the southern edge of the ERW, which includes Crested Butte Mountain, stands out as these regions are warmer than the PRISM dataset. Figure 4b shows precipitation in BSU-CFSR2 is wetter in the western regions, and drier

315 in the eastern, of the ERW in comparison against PRISM. Figure S-3 and S-4 show comparisons between PRISM and the IPM configurations and indicates no biases that are persistent across seasons. During summer, the BSU-CFSR2 simulation consistently produces more precipitation than PRISM.

Although the two-meter surface air temperature bias is evident, it doesn't vary significantly across either subgrid-scale

320 physics scheme or meteorological forcing, subsequent exploration will be predominantly focused on precipitation. The bottom row in Figure 4 shows the grid-cell standard deviation of monthly precipitation across subgrid-scale physics schemes (i.e., UCD, NCAR and BSU simulations with CFSR2 meteorological forcing – bottom left) and BSU simulation driven by different meteorological forcing datasets (ERA5, CFSR2, MERR2 and NCEP – bottom right). Similar to the conclusions drawn from Figure 3, Supplementary Figure S-4 also shows the monthly spatial standard deviations across subgrid-scale

325 physics schemes are generally greater than meteorological forcing, particularly in regions of higher-elevation during the winter season.
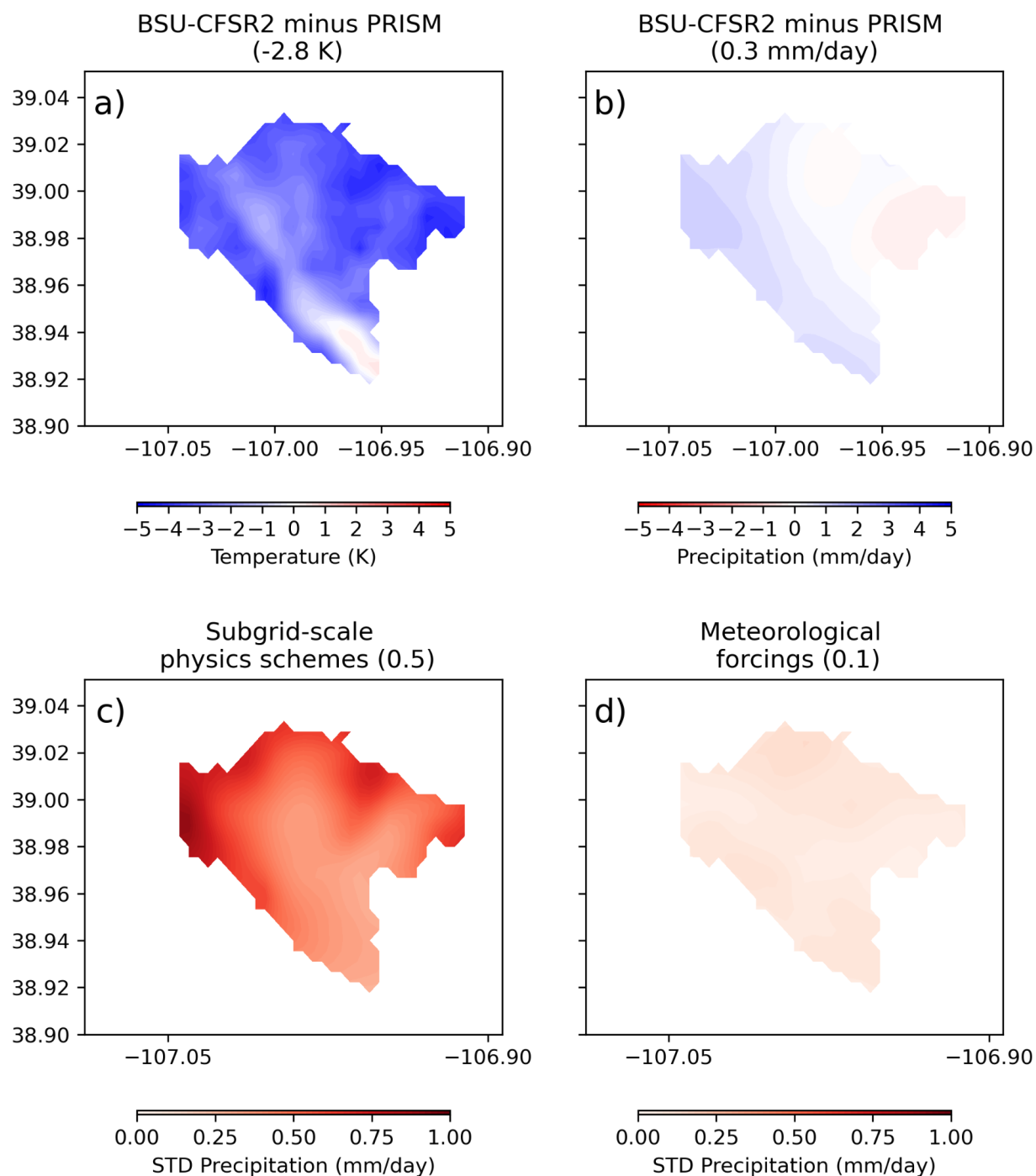
Figure 4. *Upper row: Differences in spatial distributions of annual average two-meter surface air temperature (a) and cumulative precipitation (b) between the BSU-CFSR2 WRF configuration and PRISM. Lower row: For all schemes, the*

standard deviation of annual cumulative precipitation is plotted for subgrid-scale physics schemes (c) and meteorological

forcings (d). The values in the parentheses are the domain average differences over the water year.

335   Based on the assessment of simulated precipitation and two-meter surface air temperature compared with PRISM, the BSU-

CFSR2 configuration is selected as a baseline to further explore the influence of topographic radiation scheme effects. Figure

5 shows daily ERW spatial average time series over the water year for the major mountainous water and energy budget

variables. By isolating the impacts of subgrid-scale physics schemes and meteorological forcings across IPM simulations, it

is easier to to systematically intercompare cause-and-effect across different topographic radiation options. Consistent with

340   previous findings, all configurations still overestimate cumulative precipitation and are too cold relative to PRISM.
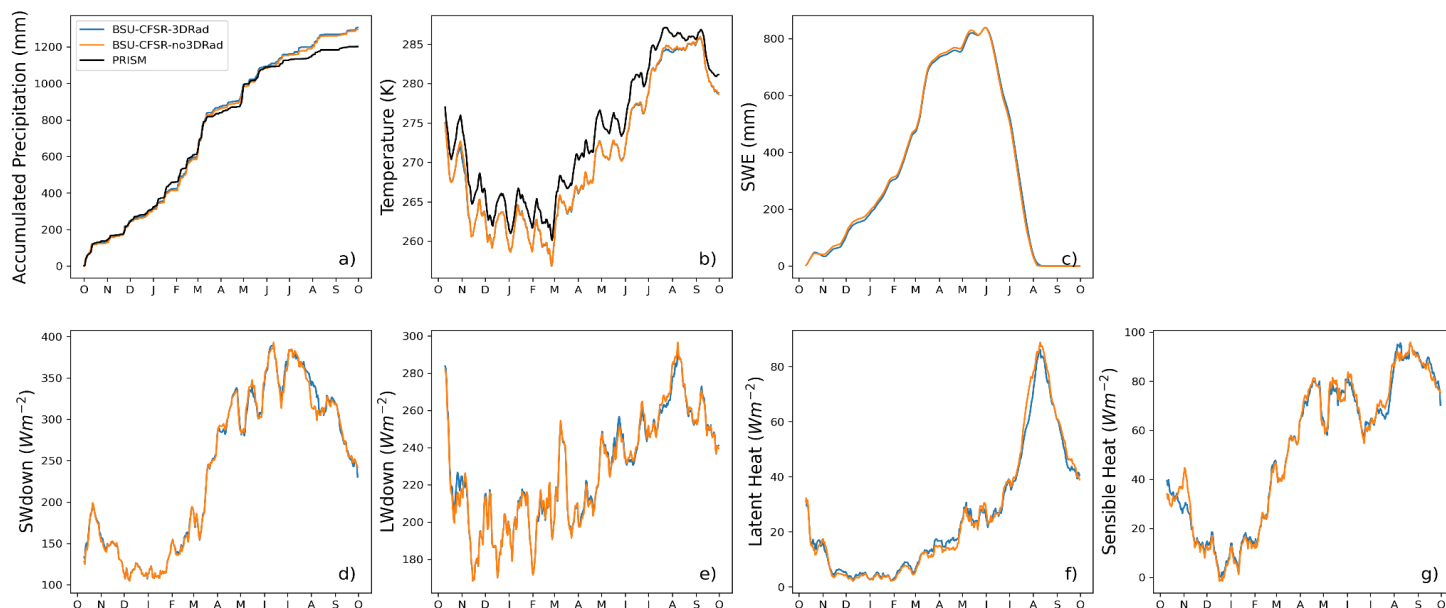
Figure 5. *Spatial-average cumulative precipitation, two-meter surface air temperature and snow water equivalent (SWE)*

(first row), shortwave and longwave radiation, and latent and sensible heat (second row) over the ERW as simulated by the

345   *IPM configurations with and without realistic topographic radiation effects, along with, where available, estimates from*

PRISM. 3DRad indicates a simulation with topo_shading and slope_rad turned on in the WRF inner domain but not the

outer WRF domains, no3DRad indicates a simulation with top_shading and slope_rad turned off in both the inner and outer

WRF domains. 10-day moving averages are shown in b) temperature, and radiation variables (d, e, f, g).

350   Figure 6 shows the seasonally-resolved shortwave radiation, two-meter surface air temperature, latent heat flux and SWE for

different configurations of shortwave radiation in the simulation with and without topo_shaing and slope_rad options in the

inner domain. While no3DRad does not adjust the SWdown, 3DRad simulation recalculates the SWdown based on the

shadows cast by nearby topography. Spatial differences in IPM-simulated shortwave radiation (Figure 6b) are seen in the
northeast and western portions of the ERW, when topographic effect of shortwave radiation is included. As a result, a
355 corresponding change in the spatial pattern of simulated two-meter surface air temperature and latent heat flux are seen,
which are driven by the change in downwelling shortwave radiation with topographic shading (Figures 6a and 6d). The
resulting pattern change in SWE (Figure 6c) shows that the northern and northeastern sections of the ERW, where snowpack
are concentrated, are sensitive to shortwave radiation. This is expected and consistent with previous findings that included
topographic effects in shortwave radiation and found distinct spatial patterns of hydrologic variable sensitivity due to both
360 shadows and surface reflection that produce time-varying effects on net surface radiation (Lee et al., 2015; Palazzi et al.,
2019; Gu et al., 2020; Hao et al., 2021).

Although Figure 5 shows that realistic shortwave radiation produces small effects on the seasonal cycle of the surface energy
and mass budgets when averaged over the entire watershed, including annual average SWE (Figure 5c), Figure 6c shows that
365 mountains and valleys have different amounts of SWE. Furthermore, seasonal patterns show simulated latent heat is
diminished at lower elevations from March to May, when snowmelt occurs in the valley, and the remaining snowpack in the
mountains and late snowmelt in 3DRad simulation causes lower latent heat flux shown in July (Figure S-5). The 3DRad
simulation has less SWE in the valleys during the accumulation season but more SWE at higher elevations during the melt
season, which is a direct result of the differences in shortwave radiation redistribution. Figure S-5 also shows that the latent
370 heat differences in north-facing and south-facing sides are most apparent in the snowmelt and warm seasons. This is
consistent with previous findings (Lee et al., 2015; Palazzi et al., 2019; Gu et al., 2020; Hao et al., 2021), that a more
realistic treatment of shortwave radiation, which includes shadows and projected insolation on sloped surfaces, results in
lower shortwave insolation on the surface at this time of year. The lower shortwave radiation should, in turn, decrease the
energy available for the IPM to produce snowmelt.
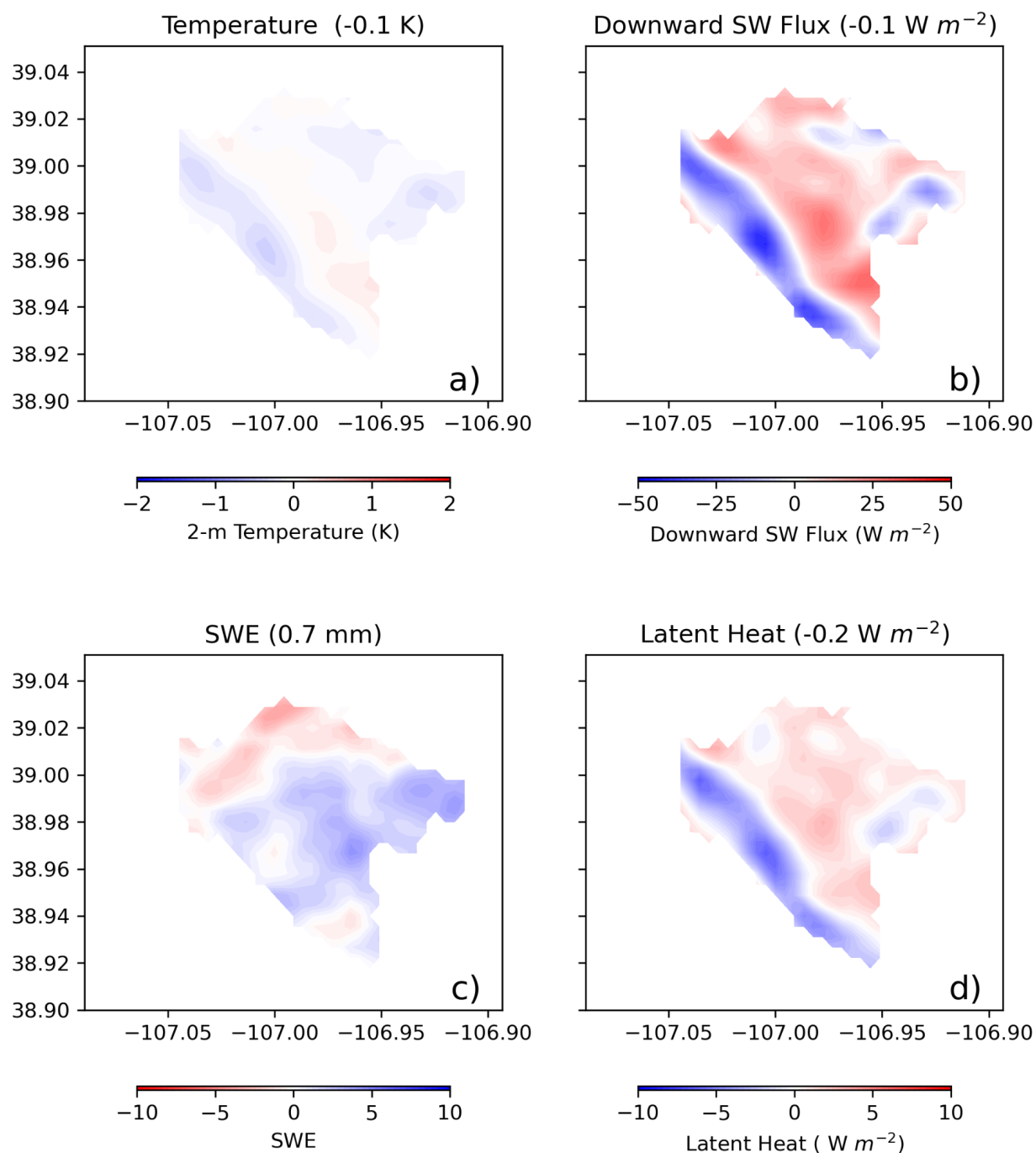
Figure 6. *Topographic radiation differences (3dRad minus no3dRad) annual average two-meter surface air temperature, shortwave (SW) and latent heat flux, and snow water equivalent (SWE) over the ERW. The values in the parentheses are the ERW average differences over the water year, which are small and consistent with Figure 5.*

380 To understand how the aforementioned WRF configurations and forcings impact the integrated water budget, Figure 7 shows the simulated hydrologic output from the ParFlow-CLM model for watershed outlet discharge (top row) and watershed-average groundwater storage (bottom row). Discharge at the watershed outlet (see exact location on Figure 1) shows general agreement across the different WRF subgrid-scale physics scheme configurations and meteorological forcings, where the daily averaged time series (left) shows only minor differences through time. However, cumulative discharge by year-end

385 reveals substantial differences (right), especially after peak snowmelt where estimates of cumulative discharge begin to diverge. Differences across the WRF configurations are especially large; the difference across the three subgrid-scale physics scheme configurations with ERA5 (UCD, NCAR, and BSU) varies by 26% by year-end. Differences across meteorological forcing (using the BSU physics configuration as a control, shown in green) are also noteworthy, although smaller, approximately 6%. These results are consistent with variation of simulated precipitation in WRF described earlier,

390 confirming that for this basin, meteorological forcing drives less variance on hydrologic response than subgrid-scale physics scheme   configuration.
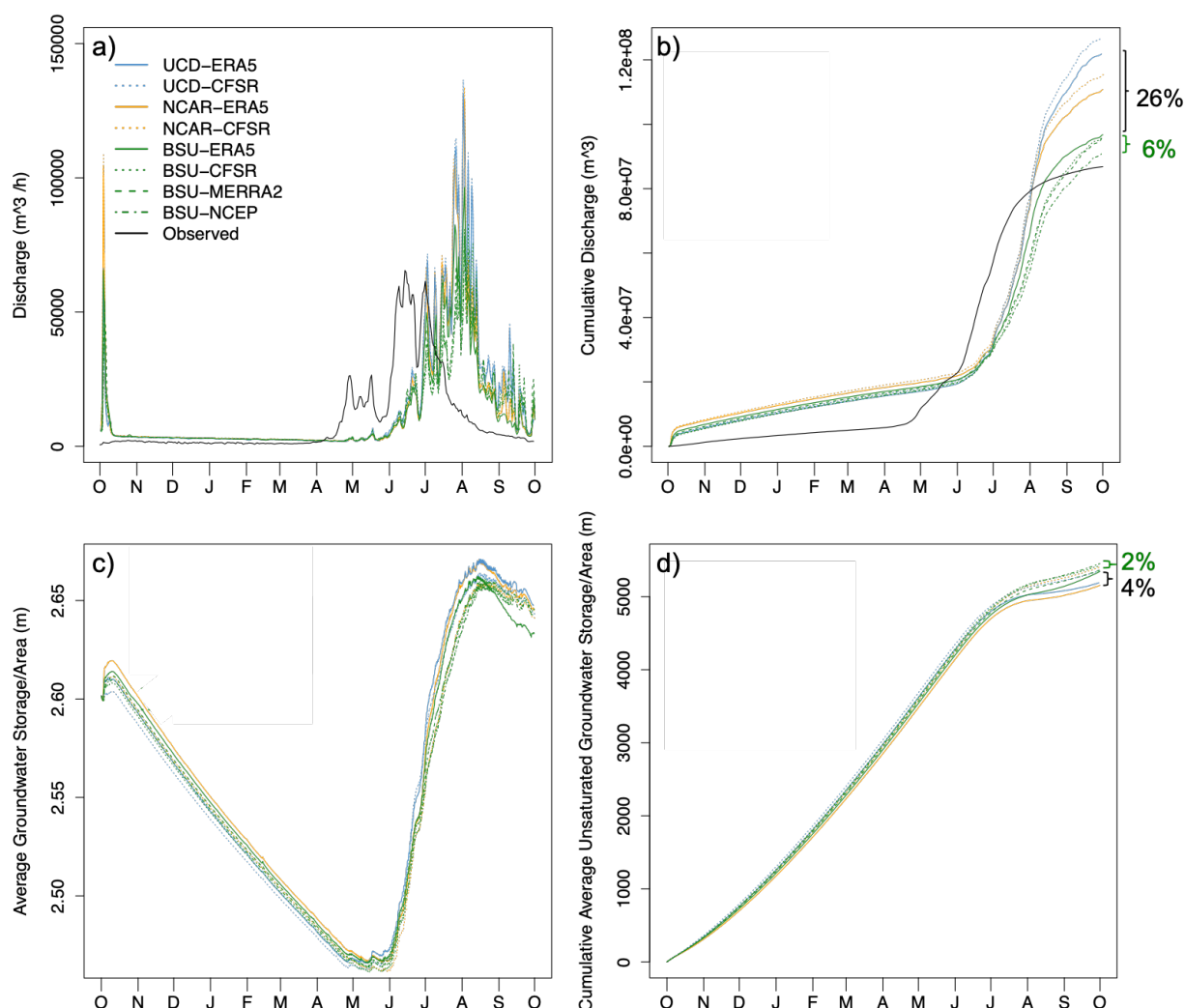
Figure 7. Time-series of ParFlow-CLM simulations of discharge rate (a), cumulative discharge (b), groundwater storage per unit area of the watershed (c), and cumulative average unsaturated groundwater storage per area of the watershed (d) for the IPM configurations described in Table 2. The brackets on the far-right indicate the percent difference of cumulative discharge and unsaturated groundwater storage per area (b and d, respectively) for WRF simulations across different meteorological forcings (green) and subgrid-scale physics schemes (black).

A comparison to observed discharge is also shown on Figure 7, which for all scenarios suggest a delayed snowmelt response in the IPM. While the objective of this study is not to replicate the observations, but rather determine sensitivity across IPM configuration choice, the mismatch in streamflow response suggests a systematic cold-bias from the WRF input into

ParFlow-CLM which is consistent with the discussion surrounding Figure 3 in relationship to PRISM. An early-fall peak in simulated discharge is also seen in all WRF simulations, and not in observed discharge, although a significant increase in

405   SNOTEL precipitation was measured in October of that year (see Figure S-1, S-2). This further supports a temperature bias, albeit opposite that of the cold-bias discussed previously, where precipitation around that October storm-event falling as rain (as opposed to snow) leads to a sharp increase in discharge. A sensitivity analysis of the BSU-ERA5 model run for a lower precipitation year (water year 2018, which was nearly half the precipitation of 2019), showed better agreement with observed discharge, which suggests the bias in timing may be a function of accumulated precipitation and/or snowmelt, and

410   is reserved for future studies (not shown).

Basin-average groundwater storage, shown in Figure 7c in area-normalized units, shows a strong annual signal for all WRF configurations with notable, but minimal differences across IPM configurations. Here all groundwater, inclusive of saturated or unsaturated storage, is considered. The cumulative, area-normalized annual groundwater storage, when accounting for

415   only vadose zone storage (Figure 7d), which is most responsive to sub-annual differences in precipitation inputs, is meaningful in this context because it relates a cumulative impact on near-surface groundwater storage due to IPM configuration. Similar to year-end cumulative discharge, year-end departures in vadose zone groundwater storage across the different simulations are evident. Differences across the IPM configurations of subgrid-scale physics schemes are slightly larger than the difference across the forcing simulations (4% versus 2%, respectively). While the differences in groundwater

420   signals are not as pronounced as the discharge signals, the slower, more muted-nature of infiltration and impacts on deeper aquifer reserves relative to discharge would likely be more notable for multi-year simulations and/or in more water-limited environments (or water years) where plant-water use demands are higher.

Figure 8 shows maps of standard deviations in annual total evapotranspiration (ET) simulated by ParFlow-CLM across IPM

425   configurations (top row), as well as the cell-binned relationship of those standard deviations of annual ET with land use and cover type, as well as elevation (bottom). Consistent with variations shown in the simulated discharge and groundwater storage, Parflow-CLM simulates greater variations of ET under WRF configurations driven by different subgrid-scale physics schemes (Figure 8a), compared to the simulations conducted with different meteorological forcings (Figure 8b). These results suggest that locations populated by high-water demanding vegetation (namely evergreen and deciduous

430   forests) at mid-elevations result in the highest ET variability across IPM configurations. Conversely, low-water demanding vegetation (barren/sparsely vegetated land and grasses), which reside across a range of elevations in the study domain, result in the lowest variability in annual ET across IPM configurations. These differences in water demand essentially magnify any differences in atmospheric conditions.
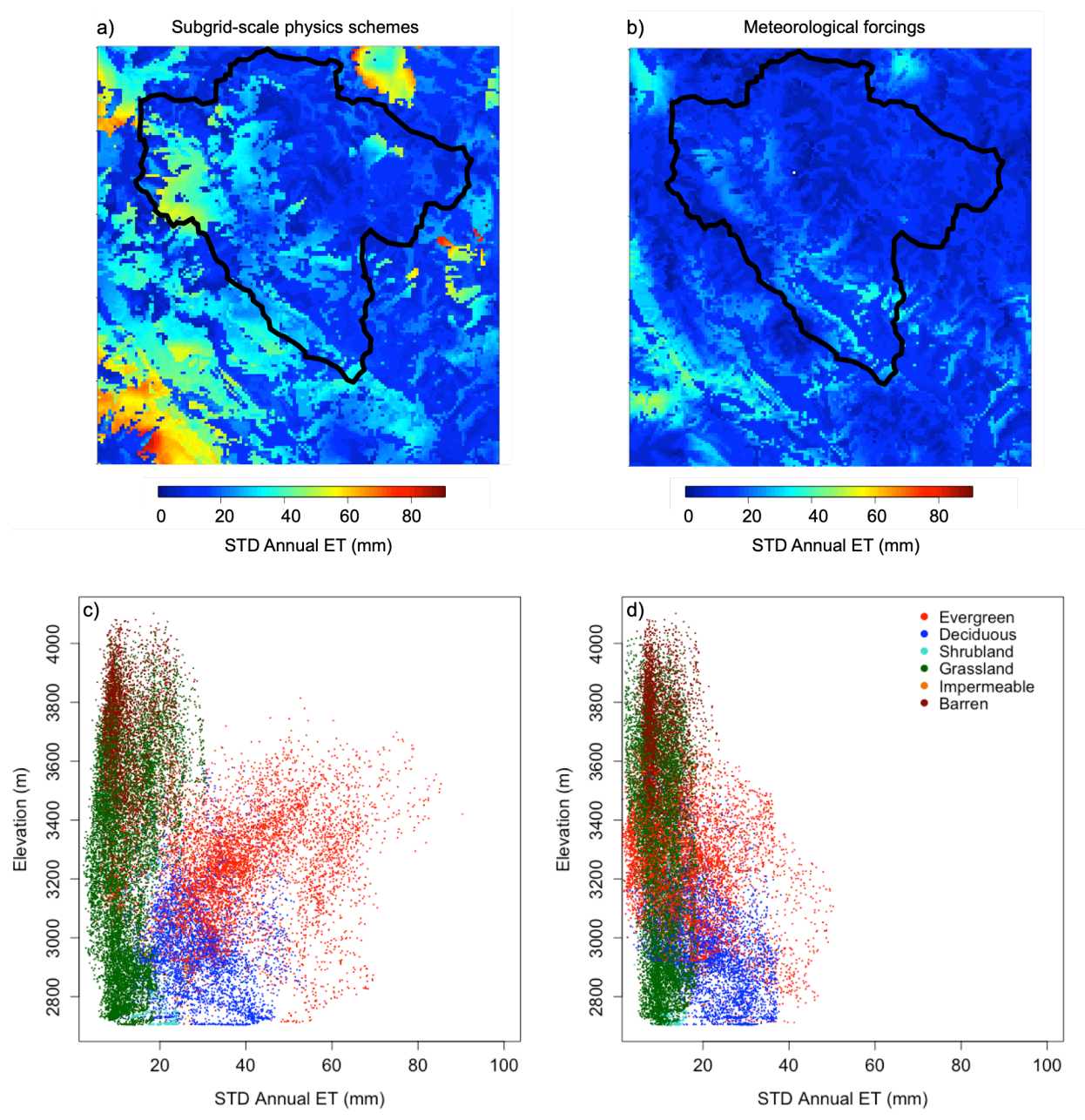
Figure 8. *Pixel-level standard deviation in annual total evapotranspiration (ET) over the ParFlow-CLM domain from WRF with different subgrid-scale physics schemes (a,c) or meteorological forcing (b,d). The ERW outline is overlain in black in the upper row, a-b. The relationship between annual ET, elevation, and land cover type are shown as scatter plots on the bottom row, c-d. See Figure 1 for maps of land cover types.*

435

5. Discussion and Conclusions

440

In spite of previous efforts to characterize the sensitivity of WRF simulations to model configuration choices, the mountain climate and hydrology scientific community has not sufficiently explored the implications of those choices for surface and subsurface hydrology in high-altitude complex terrain. Here, we used an IPM produced by coupling WRF and ParFlow-CLM to assess the hydrometeorology of the ERW which is characterized by strong hydrological gradients indicative of

445   mountain environments of the UCRB.

In this paper, we present a number of numerical experiment results that are informative for the scientific community to better understand atmosphere-through-bedrock process interactions, with an eye towards how to represent those interactions in climate and hydrological models. First, the uncertainties associated with meteorological forcing choice are less important

450   than subgrid-scale physics scheme choice, at least in the ERW. This finding has important implications for IPM in complex terrain, since it reveals that the differences in reanalysis products are less consequential for initializing and forcing IPMs than atmospheric configurations, and that efforts to advance IPMs such as collecting observations and using them to evaluate physical process parameterizations at the sub-HUC-8 scale could help to better constrain model performance. This result also shows that the boundary conditions of the IPM simulation are less important in driving the magnitude and spatial variability

455   of key hydrometeorological variables than the details in choosing and optimizing atmospheric subgrid-scale physics schemes (e.g., microphysics or boundary layer turbulence). Ultimately, we found that the BSU-CFSR2 configuration produced the most accurate recreation of WY2019 in the ERW which allows researchers, in this case, to prioritize process studies and the development of associated observational constraints within the ERW. However, further investigation is need to evaluate the systemic cold bias across IPM configurations, particularly at higher elevations, and the consequence of delayed snowmelt

460   and timing of discharge peaks.

In the investigation of topographical and slope gradient effects on shortwave radiation, our study shows those considerations in WRF are essential in redistributing radiation flux over regions of complex terrain, even though the differences in spatial-average performance over ERW is minimal. This is because the spatial redistribution of shortwave radiation leads to

465   approximately +/- 30 W/m² difference in the east/west facing slopes that lead to +/- 1 K difference in two-meter surface air temperature in August and September (when snowpack is nonexistent). Throughout most of the water year when snowpack exists, the spatial heterogeneity of temperature differences are less apparent than for shortwave radiation. Latent heat is posited to buffer differences in the shortwave radiation contribution to the radiation budget, and causes early snowmelt in the high elevation mountains in those simulations with topographical and slope gradient shortwave radiation effects turned on.

470   At the same time, this finding is potentially indicative of challenges in extrapolating findings from one mountainous watershed to another. If atmospheric process details are significant for surface and subsurface hydrological modeling and if the findings regarding atmospheric processes in one study area are marginally or completely irrelevant to other mountainous

watersheds, then additional field work would be needed in mountainous hydrology research to address this issue, given that the extrapolation of fieldwork results remains a central challenge for field-based research and modeling activities.

475

A limitation of our study, given the computational constraints of running IPMs, is that it was infeasible to explore the full parameter spaces of WRF and ParFlow-CLM exhaustively; thus, our conclusions are limited to the selected subgrid-scale physics schemes and meteorological forcing datasets analyzed. Additional work is needed to improve the systemic cold bias in two-meter surface air temperature throughout all experiments as this may have been the major driver in the delayed

480   snowmelt and peak discharge simulated by the IPM. Another methodological constraint is that our WRF and Parflow-CLM experiments were only one-way coupled instead of two-way coupled, which ignores potentially important feedbacks from the subsurface hydrology to the atmosphere via ET and the radiation budget. For example, Givati et al. (2016) reported that simulated precipitation was improved with two-way coupling in WRF-Hydro compared to WRF-only and Forrester et al. (2018) showed that boundary layer dynamics were impacted in IPM simulations in regions where shallow water tables exist.

485

Future work will include integration of data, either indirectly through IPM benchmarking or directly through data assimilation into the IPM, from a recently deployed atmospheric observatory in the ERW as part of the Surface Atmosphere Integrated Field Laboratory (SAIL) Campaign, which will run from September, 2021 to June, 2023. SAIL is collecting a wide-array of observations with the intent to advance understanding of precipitation, snow, aerosol, aerosol-cloud

490   interaction, and radiation processes in complex terrain and establish the minimum-but-sufficient level of process understanding to develop a robust predictive understanding of seasonal surface water and energy budgets in the ERW (Feldman et al., 2021). SAIL is working in conjunction with the Watershed Function Scientific Focus Area (WF-SFA) and partners including the National Oceanic and Atmospheric Administration (NOAA)'s Study for Precipitation, the Lower Atmosphere, and Surface for Hydrometeorology (SPLASH), the United States Geological Survey's Next Generation Water

495   Observing System (NGWOS), the National Science Foundation's Sublimation of Snow (SOS) project, and numerous state and local agencies and organizations, including the Rocky Mountain Biological Laboratory, to develop a wide range of hydrometeorological datasets to constrain atmosphere, surface, and subsurface processes simultaneously. Together, these resources are contributing to the establishment of a highly-instrumented and studied UCRB watershed. Our study highlights that the benchmarking provided by these data collections will be critical in addressing the systemic IPM cold bias by

500   providing a more constrained estimate of radiation budgets in complex terrain that ultimately shape snowmelt and discharge.

Data Availability: All WRF model output files can be found at

https://portal.nersc.gov/archive/home/z/zexuanxu/Shared/www/IPM

Please notify corresponding author Zexuan Xu (zexuanxu@lbl.gov) if you used our data.

505

Author contributions: ZX, ESW, AMR and DF designed the study together. ZX performed the WRF simulations and analyzed the results. ESW performed the ParFlow-CLM simulations. All authors contributed to the writing and approve of this manuscript.

510   *Competing interests:* The contact author has declared that neither they nor their co-authors have any competing interests.

Acknowledgements: This work was supported by the Laboratory Directed Research and Development Program of Lawrence Berkeley National Laboratory under U.S. Department of Energy Contract No. DE-AC02-05CH11231. This research used resources of the National Energy Research Scientific Computing Center, a DOE Office of Science User Facility supported
515   by the Office of Science of the U.S. Department of Energy under that same contract. This research also used the Lawrencium computational cluster resource provided by the IT Division at the Lawrence Berkeley National Laboratory (supported by the Director, Office of Science, Office of Basic Energy Sciences, of the U.S. Department of Energy under contract no. DE-AC02-05CH11231). The authors acknowledge the helpful guidance provided by Professor Lejo Flores and Dr. Will Rudisill of Boise State University regarding the WRF configurations conducted in this study over the ERW.

520

Financial support: First author Xu's material pertaining to WRF simulations was supported by the Laboratory Directed Research and Development Program of Lawrence Berkeley National Laboratory under U.S. Department of Energy Contract No. DE-AC02-05CH11231, and his material pertaining to the analysis using reference and observation datasets was supported by the Lawrence Berkeley National Laboratory's Watershed Function Science Focus Area of the U.S. Department
525   of Energy's Environmental System Science (ESS) Program, also under the same contract.
Co-authors Feldman and Siirila-Woodburn's material was supported by the Laboratory Directed Research and Development Program of Lawrence Berkeley National Laboratory under the same contract. Co-author Rhoades was funded by the Director, Office of Science, Office of Biological and Environmental Research of the U.S. Department of Energy Regional and Global Climate Modeling (RGCM) Program through the Calibrated and Systematic Characterization, Attribution and
530   Detection of Extremes (CASCADE) Science Focus Area and the Integrated Evaluation of the Simulated Hydroclimate System of the Continental US project also under the same contract.

References:

Arthur, R. S., Lundquist, K. A., Mirocha, J. D., and Chow, F. K.: Topographic effects on radiation in the WRF Model with the immersed boundary method: Implementation, validation, and application to complex terrain, Monthly Weather
535   Review, 146, 3277–3292, https://doi.org/10.1175/MWR-D-18-0108.1, 2018.

Ashby, S. F. and Falgout, R. D.: A parallel multigrid preconditioned conjugate gradient algorithm for groundwater flow simulations, Nuclear science and engineering, 124, 145–159, https://doi.org/10.13182/NSE96-A24230, 1996.

Comin, A. N., Schumacher, V., Justino, F., and Fernandez, A.: Impact of different microphysical parameterizations on extreme snowfall events in the Southern Andes, Weather and climate extremes, 21, 65–75,
540   https://doi.org/10.1016/j.wace.2018.07.001, 2018.

Dai, Y., Zeng, X., Dickinson, R. E., Baker, I., Bonan, G. B., Bosilovich, M. G., Denning, A. S., Dirmeyer, P. A., Houser, P. R., Niu, G., Oleson, K. W., Schlosser, C. A., & Yang, Z.: The Common Land Model, Bulletin of the American Meteorological Society, 84(8), 1013-1024, doi:10.1175/BAMS-84-8-1013, 2003.

Daly, C., Halbleib, M., Smith, J. I., Gibson, W. P., Doggett, M. K., Taylor, G. H., Curtis, J., and Pasteris, P. P.:
545   Physiographically sensitive mapping of climatological temperature and precipitation across the conterminous United States, International Journal of Climatology: a Journal of the Royal Meteorological Society, 28, 2031–2064, https://doi.org/10.1002/joc.1688, 2008.

Deems, J. S., Painter, T. H., and Finnegan, D. C.: Lidar measurement of snow depth: a review, Journal of Glaciology, 59, 467–479, https://doi.org/10.3189/2013JoG12J154, 2013.

550   Fassnacht, S., Dressler, K., and Bales, R.: Snow water equivalent interpolation for the Colorado River Basin from snow telemetry (SNOTEL) data, Water Resources Research, 39, https://doi.org/10.1029/2002WR001512, 2003.

Feldman, D.R. et al.: Surface Atmosphere Integrated Field Laboratory (SAIL) Science Plan, Ed. by Robert Stafford, ARM user facility. DOE/SC-ARM-21-004, 2021.

Forrester, M. M., Maxwell, R. M., Bearup, L. A., and Gochis, D. J.: Forest disturbance feedbacks from bedrock to
555   atmosphere using coupled hydrometeorological simulations over the Rocky Mountain headwaters, Journal of Geophysical Research: Atmospheres, 123, 9026–9046, https://doi.org/10.1029/2018JD028380, 2018.

Gelaro, R., McCarty, W., Suárez, M. J., Todling, R., Molod, A., Takacs, L., Randles, C. A., Darmenov, A., Bosilovich, M. G., Reichle, R., et al.: The modern-era retrospective analysis for research and applications, version 2 (MERRA-2), Journal of climate, 30, 5419–5454, https://doi.org/10.1175/JCLI-D-16-0758.1, 2017.

560   Givati, A., Gochis, D., Rummler, T., and Kunstmann, H.: Comparing one-way and two-way coupled hydrometeorological forecasting systems for flood forecasting in the Mediterranean region, Hydrology, 3, 19, https://doi.org/10.3390/hydrology3020019, 2016.

Gu, C., Huang, A., Wu, Y., Yang, B., Mu, X., Zhang, X., and Cai, S.: Effects of subgrid terrain radiative forcing on the ability of RegCM4. 1 in the simulation of summer precipitation over China, Journal of Geophysical Research:
565   Atmospheres, 125, e2019JD032 215, https://doi.org/10.1029/2019JD032215, 2020.

Gutowski, W. J., Jr, Ullrich, P. A., Hall, A., Leung, L. R., O'Brien, T. A., Patricola, C. M., Arritt, R. W., Bukovsky, M. S., Calvin, K. V., Feng, Z., Jones, A. D., Kooperman, G. J., Monier, E., Pritchard, M. S., Pryor, S. C., Qian, Y., Rhoades, A. M., Roberts, A. F., Sakaguchi, K., Urban, N., and Zarzycki, C.: The Ongoing Need for High-Resolution Regional Climate Models: Process Understanding and Stakeholder Information, Bulletin of the American Meteorological Society,
570   101(5), E664-E683. https://doi.org/10.1175/BAMS-D-19-0113.1, 2020.

Hao, D., Bisht, G., Gu, Y., Lee, W.-L., Liou, K.-N., and Leung, L. R.: A parameterization of sub-grid topographical effects on solar radiation in the E3SM Land Model (version 1.0): implementation and evaluation over the Tibetan Plateau, Geoscientific Model Development, 14, 6273–6289, https://doi.org/10.5194/gmd-14-6273-2021, 2021.

Hersbach, H, Bell, B, Berrisford, P, et al.: The ERA5 global reanalysis. Quarterly Journal of the Royal Meteorological
575   Society, 146, 1999– 2049, doi:10.1002/qj.3803, 2020.

Homer, C., et al.: Conterminous United States land cover change patterns 2001–2016 from the 2016 National Land Cover Database, ISPRS Journal of Photogrammetry and Remote Sensing, 162, 184-199, doi:10.1016/j.isprsjprs.2020.02.019, 2020.

Huang, X., Rhoades, A. M., Ullrich, P. A., and Zarzycki, C. M.: An evaluation of the variable-resolution CESM for
580   modeling California's climate, Journal of Advances in Modeling Earth Systems, 8, 345–369, https://doi.org/10.1002/2015MS000559, 2016.

Hubbard, S. S., Williams, K. H., Agarwal, D., Banfield, J., Beller, H., Bouskill, N., Brodie, E., Carroll, R., Dafflon, B., Dwivedi, D., et al.: The East River, Colorado, Watershed: A mountainous community testbed for improving predictive understanding of multiscale hydrological–biogeochemical dynamics, Vadose Zone Journal, 17, 1–25,
585   https://doi.org/10.2136/vzj2018.03.0061, 2018.

Ikeda, K., Rasmussen, R., Liu, C., Gochis, D., Yates, D., Chen, F., Tewari, M., Barlage, M., Dudhia, J., Miller, K., et al.: Simulation of 60 seasonal snowfall over Colorado, Atmospheric Research, 97, 462–477, https://doi.org/10.1016/j.atmosres.2010.04.010, 2010.

James, T, et al.: The economic importance of the Colorado River to the basin region. Final Rep., L. William Seidman
590   Research Institute, Arizona State University, 54, https://businessforwater.org/wp-content/uploads/2016/12/PTF-Final-121814.pdf, 2014.

Jin, J., Miller, N. L., and Schlegel, N.: Sensitivity study of four land surface schemes in the WRF model, Advances in Meteorology, 2010, https://doi.org/10.1155/2010/167436, 2010.

Jones, J. E. and Woodward, C. S.: Newton–Krylov-multigrid solvers for large-scale, highly heterogeneous, variably
595   saturated flow problems, Advances in water resources, 24, 763–774, https://doi.org/10.1016/S0309-1708(00)00075-0, 2001.

Kleist, D. T., Parrish, D. F., Derber, J. C., Treadon, R., Wu, W.-S., and Lord, S.: Introduction of the GSI into the NCEP global data assimilation system, Weather and Forecasting, 24, 1691–1705, https://doi.org/10.1175/2009WAF2222201.1, 2009.

600 Lee, W.-L., Gu, Y., Liou, K., Leung, L., and Hsu, H.-H.: A global model simulation for 3-D radiative transfer impact on surface hydrology over the Sierra Nevada and Rocky Mountains, Atmospheric Chemistry and Physics, 15, 5405–5413, https://doi.org/10.5194/acp-15-5405-2015, 2015.

Liu, C., Ikeda, K., Thompson, G., Rasmussen, R., and Dudhia, J.: High-resolution simulations of wintertime precipitation in the Colorado Headwaters region: Sensitivity to physics parameterizations, Monthly Weather Review, 139, 3533–3553, https://doi.org/10.1175/MWR-D-11-00009.1, 2011.

Liu, C., Ikeda, K., Rasmussen, R., Barlage, M., Newman, A. J., Prein, A. F., Chen, F., Chen, L., Clark, M., Dai, A., et al.: Continental-scale convection-permitting modeling of the current and future climate of North America, Climate Dynamics, 49, 71–95, https://doi.org/10.1007/s00382-016-3327-9, 2017.

Lundquist, J., Hughes, M., Gutmann, E., and Kapnick, S.: Our skill in modeling mountain rain and snow is bypassing the skill of our observational networks, Bulletin of the American Meteorological Society, 100, 2473–2490, https://doi.org/10.1175/BAMS-D-19-0001.1, 2019.

Maina, F. Z., Siirila-Woodburn, E. R., and Vahmani, P.: Sensitivity of meteorological-forcing resolution on hydrologic variables, Hydrology and Earth System Sciences, 24, 3451–3474, https://doi.org/10.5194/hess-24-3451-2020, 2020.

Mallard, M. S., Spero, T. L., and Taylor, S. M.: Examining WRF's sensitivity to contemporary land-use datasets across the contiguous United States Using Dynamical Downscaling, Journal of applied meteorology and climatology, 57, 2561–2583, https://doi.org/10.1175/JAMC-D-17-0328.1, 2018.

Maxwell, R., Condon, L., and Kollet, S.: A high-resolution simulation of groundwater and surface water over most of the continental US with the integrated hydrologic model ParFlow v3, Geoscientific model development, 8, 923–937, https://doi.org/10.5194/gmd-8-923-2015, 2015.

Maxwell, R. M.: A terrain-following grid transform and preconditioner for parallel, large-scale, integrated hydrologic modeling, Advances in Water Resources, 53, 109–117, https://doi.org/10.1016/j.advwatres.2012.10.001, 2013.

Milly, P. C. and Dunne, K. A.: Colorado River flow dwindles as warming-driven loss of reflective snow energizes evaporation, Science, 367, 1252–1255, https://doi.org/10.1126/science.aay9187, 2020.

Orr, A., Listowski, C., Couttet, M., Collier, E., Immerzeel, W., Deb, P., and Bannister, D.: Sensitivity of simulated summer monsoonal precipitation in Langtang Valley, Himalaya, to cloud microphysics schemes in WRF, Journal of Geophysical Research: Atmospheres, 122, 6298–6318, 2017.

Painter, T. H., Berisford, D. F., Boardman, J. W., Bormann, K. J., Deems, J. S., Gehrke, F., Hedrick, A., Joyce, M., Laidlaw, R., Marks, D., et al.: The Airborne Snow Observatory: Fusion of scanning lidar, imaging spectrometer, and physically-based modeling for mapping snow water equivalent and snow albedo, Remote Sensing of Environment, 184, 139–152, https://doi.org/10.1016/j.rse.2016.06.018, 2016.

Palazzi, E., Mortarini, L., Terzago, S., and Von Hardenberg, J.: Elevation-dependent warming in global climate model simulations at high spatial resolution, Climate Dynamics, 52, 2685–2702, https://doi.org/10.1007/s00382-018-4287-z, 2019.

Powers, J. G., Klemp, J. B., Skamarock, W. C., Davis, C. A., Dudhia, J., Gill, D. O., Coen, J. L., Gochis, D. J., Ahmadov, R., Peckham, S. E., et al.: The weather research and forecasting model: Overview, system efforts, and future directions, Bulletin of the American Meteorological Society, 98, 1717–1737, https://doi.org/10.1175/BAMS-D-15-00308.1., 2017.

Rahimi, S., Krantz, W., Lin, Y.-H., Bass, B., Goldenson, N., Hall, A., Lebo, Z. J., and Norris, J.: Evaluation of a Reanalysis-Driven Configuration of WRF4 Over the Western United States From 1980 to 2020, Journal of Geophysical Research: Atmospheres, 127, e2021JD035 699, https://doi.org/10.1029/2021JD035699, 2022.

640 Rasmussen, K. L., Prein, A. F., Rasmussen, R. M., Ikeda, K., and Liu, C.: Changes in the convective population and thermodynamic environments in convection-permitting regional climate simulations over the United States, Climate Dynamics, 55, 383–408, https://doi.org/10.1007/s00382-017-4000-7, 2020.

Rasmussen, R., Liu, C., Ikeda, K., Gochis, D., Yates, D., Chen, F., Tewari, M., Barlage, M., Dudhia, J., Yu, W., et al.: High-resolution coupled climate runoff simulations of seasonal snowfall over Colorado: A process study of current and
645 warmer climate, Journal of Climate, 24, 3015–3048, https://doi.org/10.1175/2010JCLI3985.1, 2011.

Rasmussen, R., Ikeda, K., Liu, C., Gochis, D., Clark, M., Dai, A., Gutmann, E., Dudhia, J., Chen, F., Barlage, M., et al.: Climate change impacts on the water balance of the Colorado headwaters: high-resolution regional climate model simulations, Journal of Hydrometeorology, 15, 1091–1116, https://doi.org/10.1175/JHM-D-13-0118.1, 2014.

Rhoades, A. M., Ullrich, P. A., and Zarzycki, C. M.: Projecting 21st century snowpack trends in western USA mountains
650 using variable-resolution CESM, Climate Dynamics, 50, 261–288, https://doi.org/10.1007/s00382-017-3606-0, 2018a.

Rhoades, A. M., Ullrich, P. A., Zarzycki, C. M., Johansen, H., Margulis, S. A., Morrison, H., Xu, Z., and Collins, W. D.: Sensitivity of mountain hydroclimate simulations in variable-resolution CESM to microphysics and horizontal resolution, Journal of Advances in Modeling Earth Systems, 10, 1357–1380, https://doi.org/10.1029/2018MS001326, 2018b.

655 Rhoades, A. M., Jones, A. D., and Ullrich, P. A.: Assessing mountains as natural reservoirs with a multimetric framework. Earth's Future, 6, 1221– 1241. https://doi.org/10.1002/2017EF000789, 2018c.

Rudisill, W., Flores, A., and McNamara, J.: The Impact of Initial Snow Conditions on the Numerical Weather Simulation of a Northern Rockies Atmospheric River, Journal of Hydrometeorology, 22, 155–167, 2021.

Skamarock, W.C., Klemp, J.B., Dudhia, J., Gill, D.O., Liu, Z., Berner, J., Wang, W., Powers, J.G., Duda, M.G., Barker,
660 D.M. and Huang, X.Y.: A description of the advanced research WRF model version 4. National Center for Atmospheric Research: Boulder, CO, USA, 145, p.145, 2019.

Saha, S., Moorthi, S., Pan, H.-L., Wu, X., Wang, J., Nadiga, S., Tripp, P., Kistler, R., Woollen, J., Behringer, D., et al.: The NCEP climate forecast system reanalysis, Bulletin of the American Meteorological Society, 91, 1015–1058, https://doi.org/10.1175/2010BAMS3001.1, 2010.

665 Schreiner-McGraw, A. P. and Ajami, H.: Impact of uncertainty in precipitation forcing data sets on the hydrologic budget of an integrated hydrologic model in mountainous terrain, Water Resources Research, 56, e2020WR027 639, https://doi.org/10.1029/2020WR027639, 2020.

Serreze, M. C., Clark, M. P., Armstrong, R. L., McGinnis, D. A., and Pulwarty, R. S.: Characteristics of the western United States snowpack from snowpack telemetry (SNOTEL) data, Water Resources Research, 35, 2145–2160,
670 https://doi.org/10.1029/1999WR900090, 1999.

Siirila-Woodburn, E. R., Rhoades, A. M., Hatchett, B. J., Huning, L. S., Szinai, J., Tague, C., Nico, P. S., Feldman, D. R., Jones, A. D., Collins, W. D., et al.: A low-to-no snow future and its impacts on water resources in the western United States, Nature Reviews Earth & Environment, 2, 800–819, https://doi.org/10.1038/s43017-021-00219-y, 2021.

Sturm, M., Goldstein, M. A., and Parr, C.: Water and life from snow: A trillion dollar science question, Water Resources
675   Research, 53, 3534–3544, https://doi.org/0.1002/2017WR020840, 2017.

Ullrich, P., Xu, Z., Rhoades, A., Dettinger, M., Mount, J., Jones, A., and Vahmani, P.: California's drought of the future: A midcentury recreation of the exceptional conditions of 2012–2017, Earth's future, 6, 1568–1587, https://doi.org/10.1029/2018EF001007, 2018

Williams, A. P., Cook, B. I., and Smerdon, J. E.: Rapid intensification of the emerging southwestern North American
680   megadrought in 2020–2021, Nature Climate Change, 12, 232–234, https://doi.org/10.1038/s41558-022-01290-z, 2022.

Xu, Y., Jones, A. and Rhoades, A.: A quantitative method to decompose SWE differences between regional climate models and reanalysis datasets. Sci Rep 9, 16520. https://doi.org/10.1038/s41598-019-52880-5, 2019.

Xu, Z., Rhoades, A. M., Johansen, H., Ullrich, P. A., and Collins, W. D.: An intercomparison of GCM and RCM dynamical downscaling for characterizing the hydroclimatology of California and Nevada, Journal of Hydrometeorology, 19,
685   1485–1506, https://doi.org/10.1175/JHM-D-17-0181.1, 2018.